

Dr. José F. García
*Departament d'Enginyeria Química i
Química Analítica*

Dr. Alex Tarancón
*Departament d'Enginyeria Química i
Química Analítica*



Treball Final de Grau

**Determination of the radioactive potassium content in bananas.
Determinació del contingut de potassi radioactiu dels plàtans.**

Joan Serra Ventura

June 2019



UNIVERSITAT DE
BARCELONA

B:KC Barcelona
Knowledge
Campus
Campus d'Excel·lència Internacional

Aquesta obra esta subjecta a la llicència de:
Reconeixement–NoComercial–SenseObraDerivada



<http://creativecommons.org/licenses/by-nc-nd/3.0/es/>

I am among those who think that science has great beauty.

Marie Curie

Després d'aquests quatre mesos d'intensa feina i plenament integrat en el món de la recerca, m'agradaria agrair a totes aquelles persones que han fet possible tirar endavant aquest treball.

Primerament, agrair els meus tutors, José F. García i Alex Tarancón, per la seva valuosa ajuda, paciència i per haver-me proporcionat totes les eines i coneixements necessaris per poder dur a terme aquest treball. També agrair a l'Héctor Bagán per la seva gran implicació i hores dedicades durant aquest temps.

Agrair també el suport incondicional que m'ha donat la meva mare, el meu pare i la meva germana durant tots aquests anys, els seus consells i la seva comprensió en els moments més difícils.

També voldria agrair els companys del grup QÜESTRAM R, tant estudiants de TFG com de Màster, per totes aquelles tardes amenes que hem passat al laboratori.

Finalment, agrair tots els bons amics que he fet durant el grau, i que de ben segur seran per tota la vida, per tots els moments i experiències viscudes que han fet d'aquests quatre anys una de les millors etapes de la meva vida.

A tots vosaltres,

Moltes gràcies.

REPORT

CONTENTS

| | |
|-----------------------------------------------------|----|
| 1. SUMMARY | 3 |
| 2. RESUM | 5 |
| 3. INTRODUCTION | 7 |
| 3.1. Overview in fruit consumption | 7 |
| 3.2. Banana mineral content | 7 |
| 3.3. Radioactivity | 8 |
| 3.3.1. Radiation sources | 8 |
| 3.3.1.1. Natural radiation sources | 8 |
| 3.3.1.2. Artificial radiation sources | 8 |
| 3.3.2. Radioactive decay processes | 9 |
| 3.3.2.1. Alpha decay (α) | 9 |
| 3.3.2.2. Beta decay (β) | 9 |
| 3.3.2.3. Gamma decay (γ) | 10 |
| 3.4. Potassium-40 | 10 |
| 3.4.1. Properties and interesting aspects | 10 |
| 3.4.2. Decay processes | 11 |
| 3.5. Radiation detection and measurement techniques | 12 |
| 3.5.1. Liquid Scintillation Counting (LSC) | 12 |
| 3.5.1.1. Scintillation detector | 12 |
| 3.5.1.2. Mechanism of liquid scintillation | 12 |
| 3.5.1.3. Quenching processes | 13 |
| 3.5.1.4. Calibration | 13 |
| 3.5.2. High Resolution Gamma Spectroscopy (HRGS) | 14 |
| 3.5.2.1. Semiconductor detector | 14 |
| 3.5.3. Geiger-Müller Counting (GMC) | 14 |
| 3.5.3.1. Gaseous ionization detector | 14 |

| | |
|-----------------------------------------------------------|----|
| 3.6. Dissemination and curiosities | 15 |
| 4. OBJECTIVES | 16 |
| 5. EXPERIMENTAL SECTION | 17 |
| 5.1. Reagents and materials | 17 |
| 5.2. Apparatus | 17 |
| 5.3. Banana sample treatment | 17 |
| 5.4. Total potassium determination | 19 |
| 5.5. Beta detection | 19 |
| 5.6. Gamma detection | 20 |
| 5.6.1. Geometries preparation | 20 |
| 5.6.2. HRGS measurements | 21 |
| 5.6.3. GMC measurements | 21 |
| 6. RESULTS AND DISCUSSION | 22 |
| 6.1. Ash content determination | 22 |
| 6.2. Total potassium determination by atomic emission | 22 |
| 6.3. ^{40}K determination by beta emission | 23 |
| 6.4. ^{40}K determination by gamma emission | 26 |
| 6.5. Simple procedure for ^{40}K determination | 31 |
| 6.6. Radiochemical techniques comparison | 34 |
| 6.7. Banana dose in humans | 35 |
| 7. CONCLUSIONS | 36 |
| 8. REFERENCES AND NOTES | 37 |
| 9. ACRONYMS | 39 |
| APPENDICES | 41 |
| Appendix 1: Diagram of the work | 43 |
| Appendix 2: LSC calibration with CH_3NO_2 | 45 |
| Appendix 3: Homogeneity test | 47 |

1. SUMMARY

Bananas are known to be a great source of potassium. One of the natural isotopes of potassium, potassium-40, turns out to be radioactive. This isotope is classified as a beta and gamma emitter and even though it only represents a 0.0117% of the total natural potassium, its presence in bananas makes this fruit to be classified as a radioactive food.

For the determination of bananas potassium-40 content different radiochemical techniques have been used depending on the nature of the radioactive emission that is desired to measure. In one hand, the liquid scintillation technique for the beta particles emission and in the other hand the high resolution gamma spectrometry for the gamma rays emission. Furthermore, it has been used a Geiger-Müller counter, whose typical use is to quickly detect radiation in working surfaces with the aim of establishing a simple ^{40}K determination method in bananas to apply in teaching environments.

The determination of ^{40}K via high resolution gamma spectrometry in a banana ashes matrix and a reduced size geometry has provided the most exact results among all the others radiochemical techniques that have been used in this work. The design and application of a simple procedure for the same determination have been successfully achieved, having been banana ashes measurements with a Geiger-Müller counter the best option.

The determination has led to the establishment of the banana activity and the radiation dose received when this fruit is ingested. In the same way, such data have been used for the comparison of daily or extreme scenarios, such as tobacco use or a nuclear plant accident, with the emitted radiation by a single banana for the purpose of raise awareness of the continuous radiation that our bodies are subjected.

Keywords: Bananas, Radioactivity, Potassium, 40K.

2. RESUM

Els plàtans són coneguts per ser una fruita rica en potassi. Un dels isòtops naturals del potassi, el potassi-40, resulta ser radioactiu. Aquest isòtop és classificat com un emissor de partícules beta i gamma i, tot i que la seva abundància sigui només del 0.0117%, la seva presència en el plàtan és la causa de que aquest sigui denominat com a un aliment radioactiu.

Per a la determinació del contingut de potassi-40 en plàtans s'han emprat diverses tècniques radioquímiques depenent del tipus d'emissió radioactiva que s'ha volgut mesurar. Per una banda, la tècnica del centelleig líquid per a l'emissió de partícules beta i, per l'altra banda, l'espectrometria gamma d'alta resolució per a l'emissió de raigs gamma. També s'ha utilitzat un altre tipus de comptador anomenat Geiger-Müller, comunament utilitzat per a una ràpida detecció de radiació en superfícies de treball, amb el propòsit d'establir un mètode simple de determinació de ^{40}K en plàtans per a la seva futura implementació en entorns docents.

La determinació de ^{40}K mitjançant la tècnica d'espectrometria gamma d'alta resolució en una matriu de cendres de plàtan i en una geometria de mida reduïda ha proporcionat els resultats més exactes d'entre totes les tècniques radioquímiques que s'han emprat en aquest treball. La posada a punt d'un mètode simple per a la mateixa determinació s'ha dut a terme satisfactòriament, havent sigut la millor opció les mesures de cendres de plàtan amb un comptador Geiger-Müller.

Aquesta determinació ha portat a l'establiment de l'activitat del plàtan i la dosi de radiació que rep un ésser humà al ingerir-lo. Tanmateix, també s'ha utilitzat aquesta dada per a la comparació d'escenaris tan quotidians, per exemple el consum de tabac, com extrems, com ara un accident nuclear, amb la radiació que emet un plàtan per tal de conscienciar a la població sobre la contínua exposició a la radiació a la que els nostres cossos estan sotmesos.

Paraules clau: Plàtans, Radioactivitat, Potassi, 40K.

3. INTRODUCTION

It's worthwhile to start this work with a preliminary contextualization of the topic at different levels: the day-to-day presence of the paper main protagonist, banana; its role and standing in our nutrition, its close relationship with radioactivity and how to measure it and finally certain curiosities that may be of interest for the reader.

3.1. OVERVIEW IN FRUIT CONSUMPTION

Fruits and vegetables are essential components in a healthy diet, also an enough daily consumption could contribute in the prevention of important diseases such as diabetes, certain types of cancer and cardiovascular diseases. Approximately 3.9 million of deaths worldwide in 2017 could be connected to a low fruit and vegetable consumption, as announced by World Health Organization (WHO) and Food and Agriculture Organization of the United Nations (FAO)(1).

It is well known the recommendation of health professionals and organizations about the consumption of 5 pieces of fruit or the equivalent of, at least, 400 g of fruit per day. A large number of reports and surveys about the Spanish population fruit consumption(2) reveal that fruit predominates above lactic products and sweets as desserts in daily meals, resulting that Canarias banana is almost always the most cheered fruit (Figure 1).



Figure 1. Canarias banana.

3.2. BANANA MINERAL CONTENT

The mineral composition of Canarias banana may vary according to different factors referred to all the stages between cultivation and consumption of the fruit: from the geography of the crops zone, including soil type or altitude; the agriculture techniques used and the transporting and storage of the product(3). All this parameters could be subject of chemometrics studies with the aim of classifying unknown banana samples into concrete defined groups.

Banana is considered one of the greatest sources of potassium in fruits, only underneath a few tropical fruits such as avocado, guava or dates(4). Potassium is responsible for several biochemical functions in human body. Hormone secretion and ion transport through the famous sodium-potassium pump and potassium channels are a few examples.

3.3. RADIOACTIVITY

It is crucial for understanding the basis of this work to make an overview of radioactivity in terms of its origin, as well as the mechanisms of its behaviour.

Radioactivity is the decay process of an unstable atomic nucleus by emitting nuclear particles, such as alpha and beta particles, or gamma rays (in other words, electromagnetic radiation), to a more stable atomic nucleus.

3.3.1. Radiation sources

Depending on whether there's human intervention or not, we can distinguish two types of radiation sources: natural sources and artificial sources(5).

3.3.1.1. *Natural radiation sources*

Within natural radiation sources, we can differentiate between cosmic radiation and terrestrial radiation.

In one hand, cosmic radiation can be described as the radiation emitted in outer space that travels long distances and is capable of reaching the Earth. Its interaction with elements present in the atmosphere brings out the so-called cosmogenic nuclides, such as ^3H and ^{14}C .

In the other hand, terrestrial radiation is defined as the one caused by mineral constituents present in the Earth since its formation: the primordial nuclides and its descendants. It comes from the three natural decay chains of ^{235}U , ^{238}U and ^{232}Th . A primordial nuclide that does not participate in one of the explained natural decay chains is ^{40}K .

3.3.1.2. *Artificial radiation sources*

Artificial radiation can be described as the radiation caused by nuclear disintegrations and radionuclides produced in devices created by humans, such as nuclear reactors as the most evident example.

Some common products of this activities that can end up in the nature by leakages or controlled releases are: ^{238}U , ^{235}U and ^{90}Sr , ordered from most to least half-life.

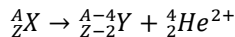
3.3.2. Radioactive decay processes

The decay process undergone by a particular nuclide depends on whether exists a proton/neutron excess or deficit, as well as the mass-energy relation of the initial and final nuclide.

It can be distinguished three types of radioactive decays: alpha decay, beta decay (positive or negative), and gamma decay(5).

3.3.2.1. Alpha decay (α)

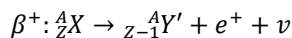
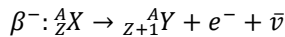
A nuclide disintegrates emitting an helium-4 particle (${}^4_2\text{He}^{2+}$) of a characteristic energy that depends on the initial nuclide. The decay can be represented as:



It is common in nuclides with a mass number (A) bigger than 150. Among its characteristics, it can be highlighted its high ionization power but low penetration effect. Thus, alpha radiation can be stopped by a simple sheet of paper.

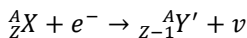
3.3.2.2. Beta decay (β)

A nuclide disintegrates emitting either an electron (beta negative, β^-) or a positron (beta positive, β^+). The decays can be represented as:



where $\bar{\nu}$ is an antineutrino and ν a neutrino. These particles were postulated by Wolfgang E. Pauli in 1927 in order to comply the conservation law of linear momentum and the total kinetic moment. Because of the null presence of e^- or e^+ in a nucleus, these processes can be explained as the transformation of a neutron into a proton emitting an electron and the antineutrino (in β^- radioactivity) or the transformation of a proton into a neutron emitting a positron and the corresponding neutrino (in β^+ radioactivity).

In a much lower probability, a nuclide can also undergo a process of electron capture (EC), where a nucleus proton captures an atomic orbital electron emitting a neutron and a neutrino. The decay proceeds as following:

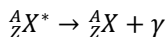


This process is in competence with β^+ decay, although the difficulties of an innermost K shell electron of being in close contact with a proton.

The beta decay process can be undergone by any type of nuclide, including a single proton or neutron and results in a continuous energy spectrum characteristic of every nuclide. It has a medium ionization power and penetration effect compared to α radioactivity. As a result, a few millimetres of lead are needed to stop β radioactivity.

3.3.2.3. Gamma decay (γ)

As a consequence of one of the radioactive decay processes explained above, a nuclide can be left in an excited state. This nuclide can return to the ground state or a lower excited state by photon emission (γ -ray, electromagnetic radiation) as shown hereunder:



The photons energy will depend in the state the nuclide returns. Since the energy states of a nuclide are discrete (quantized) and characteristic of itself, each nuclide will emit monoenergetic photons corresponding to its specific energetic transitions.

Finally, these photons are low ionizing but have a high penetration power and many centimetres of lead are required to stop them.

3.4. POTASSIUM-40

As previously announced, ${}^{40}\text{K}$ and its content in Canarias banana is the centre of this work, so it is of interest to know about the nuclide, its radioactive properties and the different decay processes that can undergo.

3.4.1. Properties and interesting aspects

${}^{40}\text{K}$ is one of the three natural isotopes (along with ${}^{39}\text{K}$ with a 93.26% abundance and ${}^{41}\text{K}$ with a 6.73% abundance) from a total of 24 potassium isotopes that are currently known(6). It can be found mostly in the earth crust or forming part of minerals, in addition to its high presence in oceans water.

It is a radioactive (unstable) isotope that only represents a 0.0117% of the total natural potassium. With one more neutron but the same atomic number ($Z=19$) in comparison with the common potassium, it results in an atomic weight of 39.96 u(6).

A half-life of $1.25 \cdot 10^9$ years (1.3 billion years, in the order of the age of the universe) makes ^{40}K a source of concern in terms of environmental care and radioactive pollution. One must take into account that it is not the only radioactive isotope of potassium, but short half-lives (ranging from milliseconds to less than a day) of these other nuclides and their artificial origin make them not considered in a study of bananas radiation.

3.4.2. Decay processes

The two types of decay processes that ^{40}K can undergo with a high probability are beta negative decay and electron capture (Figure 2).

With a 89.25% of probability, potassium-40 disintegrates by a β^- process emitting a beta negative particle (electron) with a maximum energy of 1.311 MeV and an antineutrino. As a result, ^{40}K decays to the ground state of calcium-40 (^{40}Ca)(7).

With a 10.55% of probability, ^{40}K disintegrates by electron capture followed by gamma emission (photon) of 1.460 MeV. As a result, ^{40}K decays to an excited state of ^{40}Ar (7).

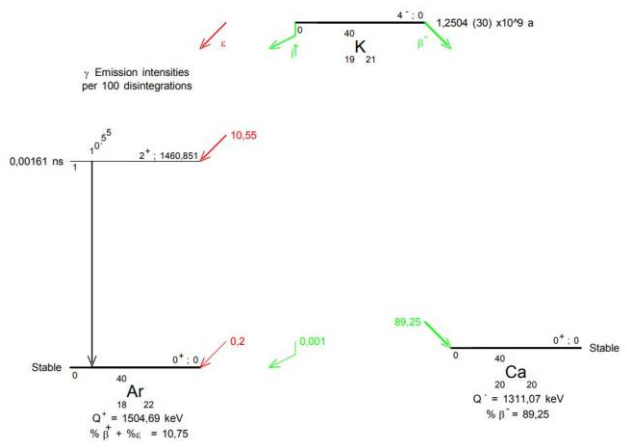


Figure 2. Potassium-40 decay chain.

(Image extracted from M.-M. Bé et al. Table of Radionuclides, 2010, 5, 7-12)

In a very small probability, ^{40}K can also disintegrate by electron capture to the ground state of ^{40}Ar (0.20%) and by beta positive emission (0.001%)(7).

3.5. RADIATION DETECTION AND MEASUREMENT TECHNIQUES

The radiochemical techniques used in this work for the determination of ^{40}K and its theoretical background are explained hereunder.

3.5.1. Liquid Scintillation Counting (LSC)

Developed in the late 40's, nowadays liquid scintillation counting (LSC) is the baseline technique for beta emitters measure, as in ^{40}K case.

3.5.1.1. Scintillation detector

The LSC is based in a scintillation detector, which measures the induced luminescence in a given compound caused by the electronic transitions to excited states and the subsequent de-excitation by photon emission.

The scintillating substances used must comply the following requirements: to be transparent in front of its own light flashes, in order to enable them to reach the photomultipliers; to emit light with a similar spectrum of that corresponding to the photomultiplier spectral sensitivity curve (typically between UV and IR zones, with a 400 nm maximum) and finally to emit a light flash that quickly decays in order to not letting detection pulses to stack, so half-life of excited states have to be short(5).

It can be distinguished two types of scintillating substances: inorganic and organic, the latter being the one used in this work.

Organic scintillating substances are able in solid and liquid state (the last ones, usually formed by dissolution of a solid scintillator in an organic aromatic solvent). Radiation excites the organic scintillator with subsequent photons emission, which reach the detector.

3.5.1.2. Mechanism of liquid scintillation

Radiation excites organic aromatic solvent molecules, transferring the energy through them, until scintillating substances (primary scintillators) are reached: the primary scintillator de-excitation is followed by photon emission, particularly in the UV zone. Usually there are another scintillating substances (secondary scintillators) that capture the emitted light and re-emit it in a higher wavelength, which is more appropriate for the photomultiplier spectral sensitivity curve(8).

The photon avalanches reach the photomultipliers where are amplified, collected and converted into electric signals. Later, they are converted into tension pulses and lastly counted and classified into a multichannel according to their amplitudes which in turn is directly related with the energy of the particle emitted in one nuclide disintegration (Figure 3).

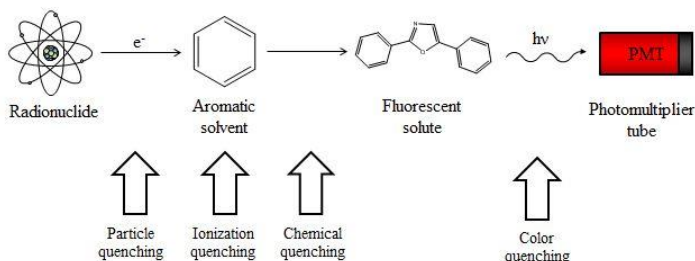


Figure 3. Detection scheme of a nuclear particle in LSC and the corresponding quench processes that can occur.

(Image extracted from Bagán H. Doctoral thesis, 2011, 28)

3.5.1.3. Quenching processes

During the energy transmission through the solvent, the scintillator and the photomultiplier it can take place a reduction or inhibition of light emission due to an interference process: quenching(9). When this phenomenon occurs, it can be expected a reduction in the detection efficiency of the method. Hereafter are explained a few quenching processes to take into consideration.

In a colour quenching process, a substance absorbs emitted photons preventing them from reaching the photomultiplier.

In a chemical quenching process, a substance affects the energy transfer from the organic aromatic solvent to the scintillator, capturing π electrons from the solvent.

3.5.1.4. Calibration

One of the most important parameters in liquid scintillation is detection efficiency (EffD),

$$\text{EffD} = \frac{\text{Net cpm}}{\text{Act}} \times 100$$

the fraction of photon avalanches counted by the detection system in relation to the total number of disintegrations produced, where "Net cpm" is the difference between the registered and the background counts and "Act" corresponds to the activity of the substance.

The most common calibration in LSC is the external calibration curve method, where detection efficiency is correlated with a parameter, the quenching parameter, obtained either from the sample spectrum or an external source.

The quenching parameters of an external source is obtained from the sample irradiation by a radioactive source (the most common is ^{152}Eu). The most used is the Spectral Quench Parameter of the External Standard, or SQP(E), which is an indicator of the uppermost channel number that comprises the integration of the 99.5% of the counts produced by the external source when it irradiates a particular sample(10).

3.5.2. High Resolution Gamma Spectroscopy (HRGS)

In the spectroscopy field of gamma radiation semiconductor detectors are typically used at the expense of inorganic scintillator detectors such as sodium iodide doped with thallium.

3.5.2.1. Semiconductor detector

In semiconductor detectors, the passage of radiation produces electron-hole pairs with their subsequent movement, which generates an electric current proportional to the deposited energy by the nuclear particle.

They are preferred for providing a high resolution that enables the interpretation of complex gamma spectrum containing various peaks. However, they offer a lower detection efficiency compared to an inorganic scintillator detector(5).

For its calibration, it has to be taken into consideration that detection efficiency will strongly depend on the geometry of the sample recipient and the sample matrix.

3.5.3. Geiger-Müller Counting (GMC)

Geiger-Müller detectors are gaseous ionization detectors that work in a particular zone of polarization.

For a better understanding of these detectors behavior, and concretely the Geiger-Müller detector, it will be done a short overview of the most important theoretical concepts.

3.5.3.1. Gaseous ionization detector

Gaseous ionization detector measures the ionization produced by a radioactive source to a gas enclosed in a chamber, which contains two electrodes working as a condenser when a

voltage is applied. The constant voltage will experiment a slight fall, that will later be measured, due to the electron-ion pairs formed during the ionization process(5).

Depending on the magnitude of the electric field intensity, the detector can work in several different ways. The Geiger-Müller detector works in the so-called Geiger zone, where the electric field intensity is such that it produces an electron avalanche due to a massive formation of electron-ion pairs. As a result, Geiger-Müller detectors cannot distinguish between charged particles or different energies.

As in the case of HRGS, for GMC calibration has to be taken into consideration that detection efficiency will strongly depend on the sample matrix and geometry used.

3.6. DISSEMINATION AND CURIOSITIES

It may be of interest to know a few facts and curious comparisons from the world of radioactivity involving bananas that will surprise the reader.

First of all, the existence of a defined magnitude named banana equivalent dose (BED) which represents the radiation dose received when a single banana is eaten. This particular magnitude was established and it is currently used to concern population about the risk of radiation exposure with a simple comparison with such a common fruit as is banana. For example, a chest computerized axial tomography (CAT) scan done in a hospital would correspond to an ingest of 70.000 bananas (7 mSv)(11). Moreover, it can be interesting for those smoker readers to know that a 1 pack of cigarettes per day habit during a whole year equates to approximately 700.000 BED (70 mSv).

A frequently asked question when talking about the radioactivity within bananas is whether its consumption is harmful to health. It will be later answered with the results obtained in this work.

4. OBJECTIVES

The main objective of this work is the development of a procedure to determine ^{40}K in bananas by radiochemical techniques. To achieve it, the following points are proposed.

First of all, the elaboration of a sample treatment plan with the aim of eliminate the interfering substances in bananas to obtain a suitable matrix to work on the further determinations.

Secondly, the total potassium determination of bananas by a spectroscopic technique such as flame emission. The following results will be referenced to the value obtained in this stage of the work.

Next, the design and application of a procedure for the ^{40}K determination of bananas by its beta and gamma emissions.

The comparison of ^{40}K activities obtained by the different radiochemical techniques to discuss possible differences obtained.

Finally, the design and application of a simple procedure for the ^{40}K determination to implement in a learning environment.

5. EXPERIMENTAL SECTION

5.1. REAGENTS AND MATERIALS

All the reagents used are of analytical grade. Hydrochloric acid fuming 37% by Merck KGaA (Darmstadt, Germany) and nitric acid 65% by Fisher Scientific (Loughborough, England) have been used to prepare the acid solution for ashes attack. Nitric acid and nitromethane (by Merck KGaA) have been used as chemical quenching agents.

For LS measurements, the scintillation cocktail Optiphase HiSafe 3 by PerkinElmer has been used.

5.2. APPARATUS

An atomic absorption/emission spectrometer AAnalyst 200 AA (by PerkinElmer) has been used for total K measurements.

A 1220 Quantulus liquid scintillation detector (by EG&G Wallac) with logarithmic amplification and a multichannel analyser of 4096 channels has been used for LS measurements (Figure 4).

A high resolution gamma spectrometer with an intrinsic germanium detector (by Canberra) has been used for gamma emissions measurements.

A LB 124 Geiger-Müller counter (by Berthold Technologies) has been used for β/γ measurements.



Figure 4. 1220 Quantulus liquid scintillation detector by EG&G Wallac.

5.3. BANANA SAMPLE TREATMENT

A representative sampling of bananas and its treatment by crushing and dry ashes method(12) previously designed (Table 1) has been done for the later determinations of total K and ^{40}K . The sample used during all the work has been the edible parts of Canarias banana from Plátano de Canarias brand, Cavendish variety with a minimum size of 16 cm.






| Stage | Image | Description |
|--------------|--------------------------------------------------------------------------------------------------------------------------------------------------------------------------------------------------------|-------------------------------------------------------------------------------------|
| Raw material |  A photograph showing several peeled banana slices stacked on a surface next to a blender jar containing banana pulp. | Banana edible part |
| Crushed |  A photograph of a blender jar filled with a smooth, light-colored banana paste, sitting on a digital scale. | Homogeneous paste after crushing |
| Carbonized |  A photograph showing three white bowls containing dark brown, charred residue from the carbonization process. | Dark brown residue after 200°C sand bath |
| Calcined |  A photograph showing three white bowls containing white, powdery ash residue after calcination. | White ashes after 500°C calcination |
| Acid attack |  A photograph showing three white bowls containing a yellowish liquid solution, representing the acid attack stage. | Ashes dissolution. Yellow coloration is due to HNO_3 thermal decomposition |

Table 1. Sample treatment stages.

Bananas have been crushed in a closed blender until achieving an homogeneous paste. 30 g of the result have been transferred into porcelain capsules. The replicates have been first heated in a sand bath at approximately 200°C and later calcined at 500°C, performing a ramp of temperatures to avoid sample inflammation. During the process temperature has not been increased beyond 500°C to prevent potassium loss(3)(13). The obtained ashes have been dissolved with 25 mL of a HCl 1:1/HNO₃ 1:1 solution and an additional 5 mL of concentrated HNO₃. To ensure the full dissolution, capsules have been heated to approximately 100°C in a sand bath.

5.4. TOTAL POTASSIUM DETERMINATION

Total potassium determination of bananas has been done by Flame Atomic Emission Spectroscopy (FAES) with few additional sample treatment steps.

Capsule contents have been filtered with ashless 110-mm filter papers (Whatman, Buckinghamshire, UK) and transferred into 250 mL flasks filled up with double deionized water(14). A volume of 2.5 mL of the solutions has been diluted to 25 mL flasks in order to reach the concentration of the technique calibration range. A concentration of 1000 ppm Na has been introduced into the measuring 25 mL flasks acting as a ionization suppressor(15).

Standards have been prepared by consecutive dilutions from a 1000 ppm K solution into a 10-80 ppm K range, containing a 1000 ppm Na concentration(15).

Blank solutions have been prepared with 2.5 mL of HCl 1:1/HNO₃ 1:1 solution, a 1000 ppm Na concentration and filled up with double deionized water.

Measurements have been performed at the emission wavelength of 776.5 nm(15)(16).

5.5. BETA DETECTION

For ⁴⁰K determination by beta emissions, LSC with a calibration method by chemical quenching, using HNO₃ and CH₃NO₂, has been described and tested for banana ashes solution matrix.

LS sample vials have been prepared by adding 6 mL of 250 mL flasks prepared in Section 5.4. and filled up with 14 mL of scintillation cocktail(17) (Figure 5). Each sample vial has been measured for 5 h with 20 min of SQP(E).

LS standard vials for chemical quenching calibration have been prepared with increasing amounts of HNO_3 or CH_3NO_2 (0-1000 μL and 0-25 μL ranges, respectively), 1 mL of a 0.3 g KCl/mL solution, 14 mL of scintillation cocktail and filled up with double deionized water to 20 mL. Each standard vial has been measured for 2 h with 20 min of SQP(E).

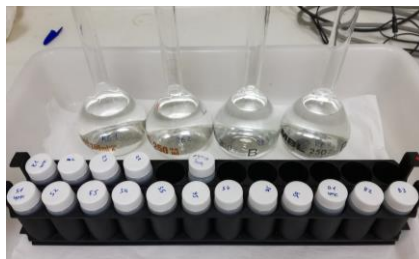


Figure 5. LS measured vials and 250 mL flasks prepared in Section 5.4.

LS blank vials have been prepared by adding increasing amounts of HNO_3 or CH_3NO_2 (same ranges than standard vials), 14 mL of scintillation cocktail and filled up with double deionized water. Each blank vial has been measured for 5 h with 20 min of SQP(E).

5.6. GAMMA DETECTION

HRGS and GM measurements for ^{40}K determination have been done for crushed banana and ashes matrices.

5.6.1. Geometries preparation

A sample geometry and a sample geometry spiked with KCl have been prepared for detection efficiency calibration of the techniques.

For crushed banana geometries (GA1 and GB1), two 500 mL geometries (Figure 6) have been filled achieving the same weight and height of sample inside the recipient. GA1 only contained crushed banana and GB1 has been prepared by adding consecutive layers of crushed banana and dried KCl (a total of approximately 30 g) with the aim of obtaining an homogeneous sample.



Figure 6. On the left, GA1. On the right, GB1.

For the preparation of banana ashes geometries (GA2 and GB2), previous geometry contents have been treated as indicated in Section 5.3. and ashes obtained have been disposed in optimised geometries (100 mL geometry covers, Figure 7), achieving the same weight and height,



Figure 7. On the left, GA2 geometry. On the right, GB2 geometry.

which have been covered with parafilm. GA2 and GB2 have been prepared from GA1 and GB1, respectively (Appendix 1).

5.6.2. HRGS measurements

GA1 and GA2 geometries have been measured for 3 days. GB1 and GB2 geometries have been measured for 1 day due to the higher activity caused by the KCl addition in both geometries.

Detection efficiency calibration of the instrument, as a function of the gamma decays ratio and its energies, has also been done by Servei d'Anàlisis Isotòpiques (Universitat de Barcelona).

5.6.3. GMC measurements

Geometries have been placed in the centre of the GMC detection surface and measured for 5 h each (Figure 8). In the case of crushed banana matrix, measurements have been performed with and without the geometry cover and an alternative rectangular geometry with a bigger surface have been tested.

Background radiation measurements have been performed with an empty 500 mL geometry and an empty optimised geometry for crushed banana and ashes matrices, respectively.



Figure 8. On the left, β/γ counts per second are shown in the GM screen. On the right, set up for crushed banana geometries measurement.

6. RESULTS AND DISCUSSION

In the next sections results obtained for ash content determination, total potassium determination by atomic emission measures, ^{40}K determination by beta emission measures by LSC and by gamma emission measures by HRGS are discussed, in addition to the results obtained for the simple procedure designed for ^{40}K determination by gamma emission using GMC.

6.1. ASH CONTENT DETERMINATION

As a previous step to the total K and ^{40}K determinations, the banana ash content has been determined and a suitable matrix has been achieved, in addition to the ^{40}K preconcentration.

For ash obtainment, a calcination step of the sample at 500°C has been performed in order to eliminate the organic matter and humidity within bananas (Table 2).

| Capsule | Crushed banana mass (g) | Banana ashes mass (g) | Ash content (%) |
|---------|-------------------------|-----------------------|-----------------|
| RE1 | 30.15 | 0.3072 | 1.02 |
| RE2 | 30.05 | 0.3280 | 1.09 |
| RE3 | 30.06 | 0.3120 | 1.04 |

Table 2. Crushed banana mass and banana ashes mass obtained for ash content determination. The replicates has been used for the posterior FAES and LSC analyses.

A significant reduction in sample dimension has been observed (Table 2) after calcination mostly due to the high humidity content of bananas(18), mainly remaining metal oxides and carbonates, resulting in an average ash content of 1.04% (0.03) (RSD=3%).

6.2. TOTAL POTASSIUM DETERMINATION BY ATOMIC EMISSION

For the later comparison of the different techniques used in this work, total potassium content of bananas has been determined by FAES.

The 776.5 nm emission spectral line has been chosen in a range of concentrations from 10 to 80 ppm K for the sample and standards.

For the technique calibration an external calibration curve has been obtained with a linear fit, that follows the equation

$$y = 404.527x + 6860.77 \quad R^2 = 0.9662$$

Table 3 shows the total K concentration per 100 g of banana calculated for the samples prepared.

| Sample | [K] (mg/L) | Emission (a.u.) | [K]/100 g banana (mg/100 g) |
|--------|------------|-----------------|-----------------------------|
| 1 | 60.21 | 31218 | 494.3 |
| 2 | 60.87 | 31483 | 504.6 |
| 3 | 58.08 | 30355 | 487.7 |

Table 3. Potassium concentration, emission energy and potassium concentration per 100 g of banana of samples prepared.

The total K concentration per 100 g of banana calculated has been 496 mg K/100 g (9) (RSD=2%).

The total K concentration has been compared with data found on bibliography about Plátano de Canarias, which has been 385 mg K/100 g banana(19). Differences has been observed, probably caused by the differences between banana crops (Section 3.2.), but results are in the same order of magnitude. Thus, FAES result obtained has been taken as the reference value for comparisons throughout the posterior determinations.

6.3. ⁴⁰K DETERMINATION BY BETA EMISSION

At this point, the ⁴⁰K content in bananas has been determined by its beta emissions using LSC.

The technique calibration has been first performed with the addition of increasing volumes of HNO₃ in the measuring vials, which is present in the samples, in order to correct the possible quenching processes occurring in the matrix. Due to the results obtained, a calibration with CH₃NO₂, which is known to be a chemical quenching agent(20), has been performed.

Figure 9 shows the SQP(E) values of standards proportioned by the instrument and the corresponding detection efficiencies calculated for the calibration with HNO₃.

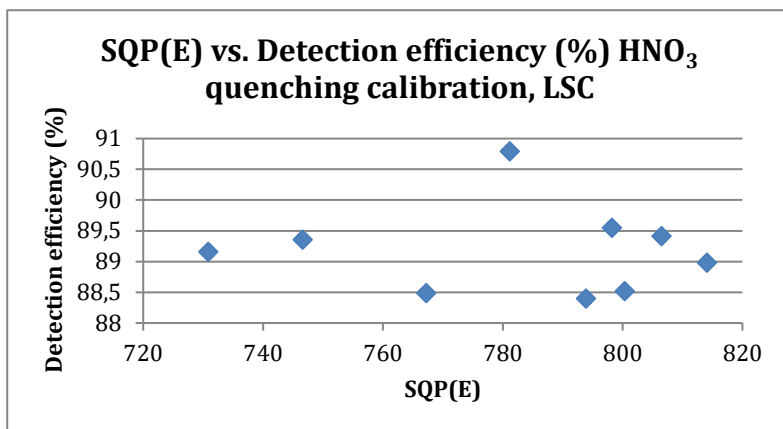


Figure 9. SQP(E) quench calibration curve representation for increasing volumes of HNO₃.

Even though it had been thought that HNO₃ could cause colour quenching by its thermal decomposition to NO₂ or by nitration of the scintillation vial plastic, no yellow colour has been observed in the samples. The calibration curve has shown a constant trend in detection efficiency of 89.2% (0.7) (RSD=0.8%) regardless the different SQP(E) values, situated in a range of 731 to 814, which indicates that HNO₃ has been acting as a chemical quenching agent. Thus, a polynomial fit has not been shown.

Figure 10 shows the spectra obtained for standard vials prepared with different HNO₃ volumes.

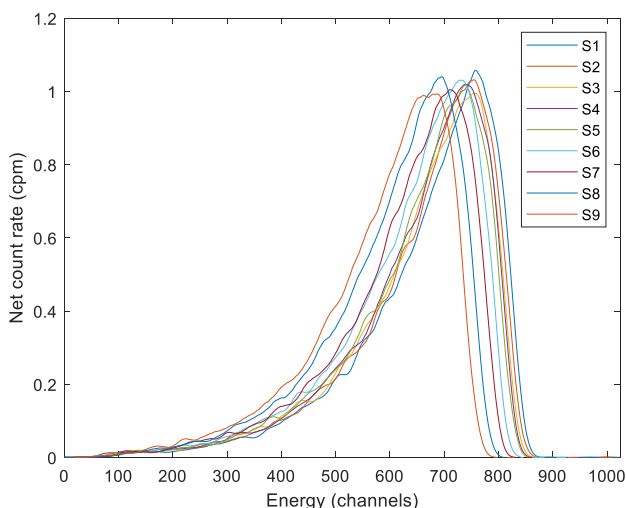


Figure 10. Spectra of the energy in every channel in front of the count rate of the standard vials containing HNO₃, from S1 to S9.

Even when the quenching causes the shift of the spectra to lower energies (in channels), caused by the increasing volumes of HNO_3 in standards (S1 does not contain HNO_3 and S9 contains the maximum HNO_3 amount), it has been proved to not be enough to see a loss of count rate in the low energy part of the spectra (channels from 0 to 100) and hence a decrease in detection efficiency. It is due to the high energy of the beta particles that ^{40}K emits, most of them appearing in channels from 600 to 800.

As HNO_3 has been proved to not produce such quench to see changes in detection efficiency, CH_3NO_2 has been used to calibrate the chemical quenching effects present in the matrix.

Even though CH_3NO_2 nitro electronegative group presence, which captures the π electrons associated with the scintillation cocktail aromatic solvent reducing the energy transfer from the beta emission, same results has been observed than the ones obtained for HNO_3 calibration: a constant trend in detection efficiency of 91.7% (0.9) (RSD=1%) regardless the different quenched standards situated in a range of 770 to 815 SQP(E) values. The shift of the spectra to lower energies for increasing volumes of CH_3NO_2 is even lower than the one observed in HNO_3 . Therefore, the constant detection efficiency of 91.7% obtained by CH_3NO_2 calibration has been selected for the posterior samples measuring (Appendix 2).

Figure 11 shows the sample spectra obtained and Table 4 includes the SQP(E) and net count rate values for each sample vial.

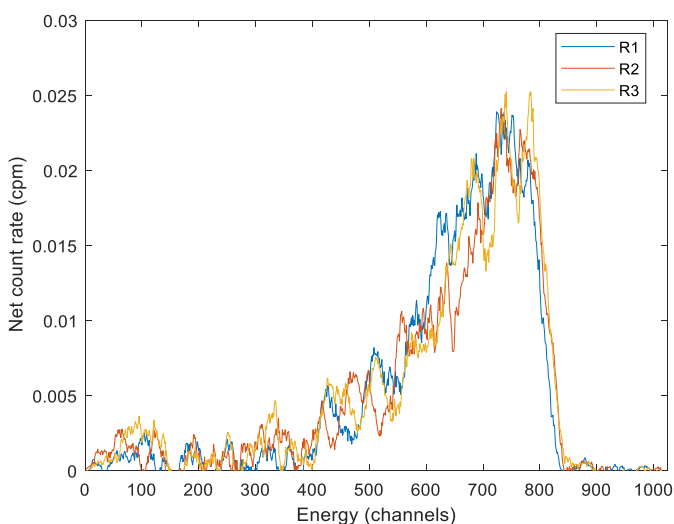


Figure 11. Spectra of the energy in channels in front of the count rate for the sample replicates.

The sample spectra has been situated in the 600-800 channels window and no other interfering peaks corresponding to different radionuclides has been observed. Even though a Savitzky-Golay smoothing has been applied, fluctuations in the sample spectra have been observed due to its count rate order of magnitude in comparison with the one for standards.

Table 4 shows the ^{40}K concentration and the deduced total K concentration in the samples prepared, as well as the SQP(E) values and the net count rate obtained for each replicate.

| Sample | SQP(E) | Net count rate (cpm) ^(a) | Activity per 100 g of banana (Bq/100 g) | [K] per 100 g of banana (mg/100 g) |
|--------|--------|-------------------------------------|-----------------------------------------|------------------------------------|
| 1 | 796.3 | 5.181 | 13.02 | 411.2 |
| 2 | 803.2 | 5.119 | 12.91 | 407.6 |
| 3 | 805.4 | 5.337 | 13.45 | 424.8 |

(a) Net count rate has been obtained by subtracting the integrated, average counts obtained of the three blanks prepared from the count rate measured for each sample vial. Average blank count rate = 3.297 cpm.

Table 4. Calculated ^{40}K and total K concentrations in the replicates. In addition, SQP(E) and net count rate values proportioned by 1220 Quantulus have been shown.

The average SQP(E) value obtained for the replicates has been approximately of 802, inside the calibration range of SQP(E) values obtained, which has indicated a low HNO_3 concentration and hence a low quenching effect in the samples.

The ^{40}K activity calculated per 100 g of banana has been 13.1 Bq/100 g (0.3) (RSD=2%) and the total K concentration per 100 g of banana has been 415 mg/100 g (9) (RSD=2%).

High precision in the ^{40}K determination results have been observed for the LSC measurements of banana ashes solution. The result obtained for total K concentration per 100 g of banana deduced from the ^{40}K determination by LSC has been close to the reference value of 496 mg/100 g obtained for total K concentration by FAES. Closer results to the total K concentration obtained by FAES were expected due to the clean matrix used, banana ashes solution, with no signal attenuation caused by the density component, in addition to the non geometry dependence of LSC in comparison with the other radiochemical techniques that have been used in this work.

6.4. ^{40}K DETERMINATION BY GAMMA EMISSION

The second technique that has been tested for the ^{40}K determination has been HRGS. The results obtained for HRGS measurements of ^{40}K gamma emissions of crushed banana and

banana ashes matrices are shown hereunder along with the technique calibration that has been performed.

Crushed banana geometries have been prepared by duplicate, one of them spiked with solid KCl standard for the technique detection efficiency calibration. Dried KCl has been used as the standard instead of a radioactive ^{40}K standard because the same geometries for HRGS measurements have been used for the later simple procedure for ^{40}K determination, whose objective is to be implemented in teaching environments where radioactive standards presence is not common. Heterogeneities in the crushed banana matrices, probably caused by encapsulated air between crushed banana layers, have been observed even though it has been tried to achieve geometries as much homogeneous as possible (Appendix 3).

After its measurement, a calcination step has been performed over the geometry contents to obtain the next ashes geometries, in order to minimise matrix effects.

Gamma spectrum of crushed banana (GA1) and crushed banana spiked with KCl (GB1) geometries obtained are shown in Figure 12 and 13, where gamma emission energies have been represented in front of the count rate registered (pulses/min).

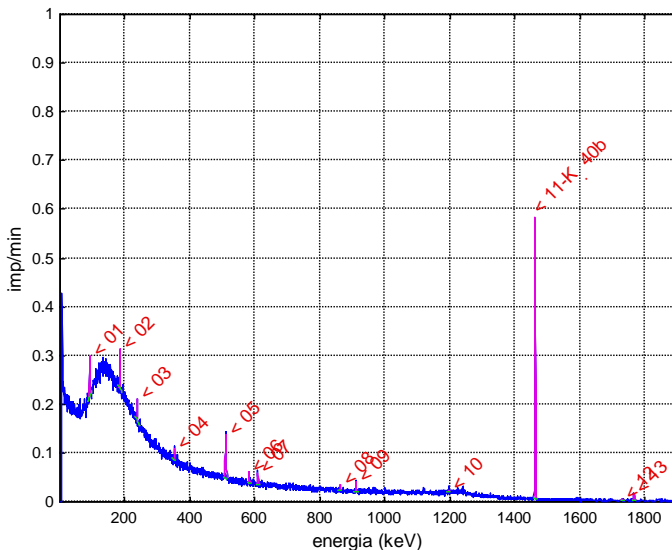


Figure 12. Representation of the gamma emissions of GA1 geometry containing crushed banana.

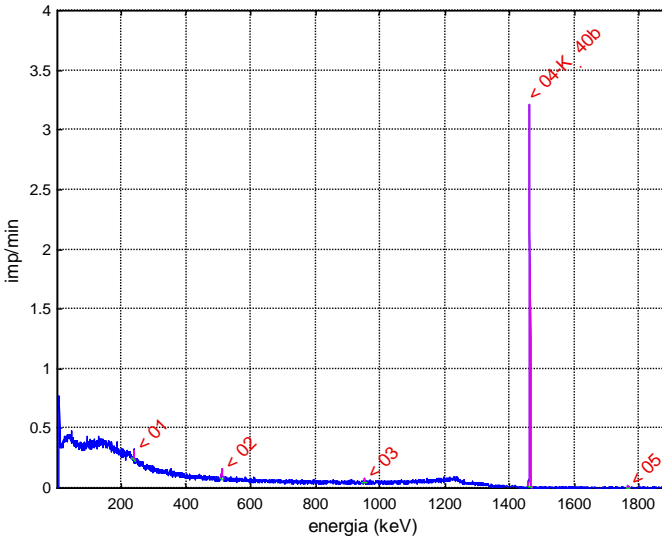


Figure 13. Representation of the gamma emissions of GB1 geometry containing crushed banana and spiked with KCl.

The gamma emissions corresponding to the ^{40}K decay to the 1460 keV excited state of ^{40}Ar by electron capture have been observed in the spectra at 1460.75 keV in both cases, giving a higher net count rate in the case of GB1: $2.78 \cdot 10^{-1}$ pulses/s in front of the $4.67 \cdot 10^{-2}$ pulses/s of GA1 and a total activity of 592 Bq for GB1 in front of the total activity of 99 Bq corresponding to GA1, all due to the KCl mass that has been added into the geometry. Since the technique only registers the gamma disintegrations, count rates have been clearly lower in comparison with the ones registered in LSC, where beta negative emissions have been registered, due to the 10.55% probability of gamma emissions in front of the 89.25% probability of beta negative emissions in the case of ^{40}K .

The second more intense peak that has been observed at 511 keV corresponds to a photon emission by a positron annihilation, procedure that happens with only a 0.002% probability. This peak have been only seen in GA1 spectrum due to the intensity relation with the ^{40}K peak. No more significant peaks corresponding to other natural radionuclides have been observed, hence the radiation within banana sample has been assumed to be caused only by ^{40}K .

The spiked geometry (GB1) has been used for the detection efficiency calibration and therefore the calculation of the crushed geometry (GA1) ^{40}K content and total K concentration deduced (Table 5).

| Geometry | Net count rate (pulses/s) ^(a) | Activity per 100 g of banana (Bq/100 g) | [K] per 100 g of banana (mg/100 g) |
|----------|---------------------------------------------|--------------------------------------------|---------------------------------------|
| GA1 | $4.667 \cdot 10^{-2}$ | 18.05 | 570.0 |

(a) Net count rate has been obtained by subtracting the background contribution to the measure, which turned out to be 0.165 pulses/min.

Table 5. ⁴⁰K and total K concentration results calculated from HRGS measurements of crushed banana matrix for the crushed banana geometry (GA1). In addition, the net count rate for the geometry has been shown.

The detection efficiency of the technique has been calibrated for the 500 mL geometry and the crushed banana matrix, resulting in a value of 0.44%. It has been slightly higher from the calibrated by Servei d'Anàlisis Isotòpiques (Universitat de Barcelona), whose value has been of 0.40%, due to the lower density of crushed banana matrix in front of water and soil matrices that they have been used for the geometry calibration procedure.

For HRGS measures of crushed banana, ⁴⁰K activity calculated per 100 g of banana has been 18.1 Bq/100 g and the total K concentration deduced from the geometry ⁴⁰K content has been 570 mg/100 g.

The ⁴⁰K activity obtained for the HRGS measurements of the crushed banana geometry has been of the same order of magnitude and hence comparable with the one obtained with LSC (13.1 Bq/100 g). Nevertheless, the total K concentration deduced from the ⁴⁰K content obtained has been far different from the one obtained by FAES (496 mg K/100 g banana) and even more for the obtained by LSC (415 mg K/100 g banana), hence has not been comparable. Differences between techniques have been attributed to crushed banana matrix attenuation of gamma emissions and geometry size, whose height has not allowed gamma rays from the top content to be emitted in an angle capable to reach the detection window of the HRGS germanium detector.

After the crushed banana measures, contents of both crushed banana and crushed banana spiked with KCl geometries have been calcined and ashes obtained have been placed in optimised geometries with a much lower height (100 mL geometry cover) protected with a semi-transparent, flexible film (Parafilm). Differences between ashes coloration have been attributable to a possible impurity from KCl (Figure 7).

Ashes geometry (GA2) and ashes geometry spiked with KCl (GB2) have come from GA1 and GB1, respectively. As in the previous case, the spiked geometry has been used for the

detection efficiency calibration of the geometry and the ashes matrix and therefore the ^{40}K and total K concentrations of the ashes geometry (Table 6).

| Geometry | Net count rate (pulse/s) ^(a) | Activity per 100 g of banana (Bq/100 g) | [K] per 100 g of banana (mg/100 g) |
|----------|--------------------------------------------|--------------------------------------------|---------------------------------------|
| GA2 | 0.1656 | 13.07 | 475.1 |

(a) Net count rate has been obtained by subtracting the background contribution to the measure, which turned out to be 1,207 pulses/min.

Table 6. ^{40}K and total K concentration results calculated from HRGS measurements of banana ashes matrix for the banana ashes geometry (GA2). In addition, the net count rate for the geometry has been shown.

The calibrated detection efficiency for the optimised geometry and the banana ashes matrix has turned out to be higher than the one calibrated for the crushed banana geometry, specifically of 1.75%. It has been attributed to the great reduction in geometry volume, achieving a lower height and hence having the most part of the sample in close contact with the germanium detector window, and the change from crushed banana to banana ashes matrix, which has provided a lower attenuation of the ^{40}K gamma emissions. It has not been compared with Servei d'Anàlisis Isotòpiques because they do not usually use 100 mL geometry covers as a geometry for HRGS measurements and therefore they do not have data registered for its calibration.

Gamma emissions corresponding to ^{40}K have appeared at 1460.75 keV and the net count rate obtained has been, as expected, higher for the spiked geometry in comparison with the banana ashes geometry (approximately 90 Bq of GB2 in front of the 63 Bq corresponding to GA2).

For HRGS measurements of banana ashes, ^{40}K activity calculated per 100 g of banana have been 13.1 Bq and the total K concentration deduced from the geometry ^{40}K content has been 475 mg/100 g.

The ^{40}K activity per 100 g of banana obtained for banana ashes measurements using HRGS has been identical to the one obtained for LSC (13.1 Bq/100 g) and very similar, hence comparable, to the results obtained for the crushed banana matrix measurements by the same technique, HRGS (18.1 Bq/100 g). The total K concentration per 100 g of banana deduced has resulted to be the closest to the one obtained by FAES measurements (496 mg/100 g). This satisfactory results have been attributed to geometry size reduction and decrease of matrix attenuation of gamma emissions due to the crushed banana calcination. The whole set of

advantages and precise results obtained have made the gamma emission measurement of banana ashes by HRGS the best technique for the ^{40}K determination in bananas among the radiochemical techniques that have been used in this work.

6.5. SIMPLE PROCEDURE FOR ^{40}K DETERMINATION

Finally, the same crushed banana and banana ashes geometries from HRGS measurements have been measured with a routine use Geiger-Müller Counter (GMC), which is not specific for radiochemical analyses, in order to establish a simple procedure for ^{40}K determination in bananas that could be implemented into teaching environments. The detection efficiency calibration has been done by the same procedure than the one employed for HRGS measurements: the spiked geometry with KCl has been used for the detection efficiency calibration of the geometry and the matrix for GMC measurements for subsequently determine the ^{40}K concentration in the non-spiked geometry.

The results obtained for GMC measurements of ^{40}K gamma emissions of crushed banana and banana ashes matrices are shown hereunder along with the technique calibration that have been performed.

Since most of the beta particles do not reach the detection surface because of their penetration effect, one may assume the count rate obtained is mainly due to gamma emissions only. Nevertheless, for crushed banana matrix, GMC measurements have been performed with and without geometry covers to see whether the change causes a filter effect on beta particles.

GMC have proportioned the β/γ count rate of the geometry contents (Table 7). For the filled geometries, the instrument has only been capable to measure the emissions from the top of the geometry, concretely the surface of the sample. In the case of background, when measures have been performed with covers, the GMC has been measuring the plastic material of the cover, while when measures have been performed without covers the GMC has been measuring the radionuclides present in the air that have been encapsulated inside the geometry.

| Geometry^(a) | β/γ count rate (cps) |
|-------------------------------|---------------------------------------------------|
| Background w/o c | 9.13 |
| Background w/ c | 7.85 |
| GA1 w/o c | 8.58 |
| GA1 w/ c | -(b) |
| GB1 w/o c | 9.26 |
| GB1 w/ c | 8.70 |

(a) w/o c = measure performed without geometry covers. w/ c = measure performed with geometry covers.

(b) Measures for GA1 geometry with cover have not been performed because results obtained for the other geometry measures were not satisfactory.

Table 7. Count rate measured for the background and filled GA1 and GB1 geometries.

The crushed banana spiked geometry (GB1) has given close but higher count rates compared to the ones for the background radiation, regardless the cover presence or not. The crushed banana geometry (GA1) has given non satisfactory results: lower count rate than the background has been obtained for measures without cover and measures with cover have not been performed because worse net results have been expected.

A rectangular 400 mL geometry filled with crushed banana, which has got a bigger surface for gamma detection, has been tested to improve the results but again same or lower count rates than the background have been obtained.

The big volume that has represented a crushed banana full filled 500 mL geometry has not allowed gamma emissions to reach the GMC detection surface. Hence, a reduction of the geometry size and sample volume has been needed in order to obtain relevant results.

Consequently, calcination of geometry contents has been done for banana ashes geometries preparation and the posterior GMC measurements. Results of the β/γ count rate registered and ^{40}K activity calculated, along with the total K concentration deduced from ^{40}K content, are shown in Table 8.

| Geometry | β/γ net count rate (cps)^(a) | Activity per 100 g of banana (Bq/100 g) | [K] per 100 g of banana (mg/100 g) |
|-----------------|---------------------------------------------------------------------|------------------------------------------------|-------------------------------------------|
| GA2 | 5.18 | 11.4 | 373.7 |

(a) Net count rate has been obtained by subtracting the background contribution to the measure, which turned out to be 9 cps for an empty optimised geometry covered with Parafilm.

Table 8. ^{40}K and total K concentration results calculated from GMC measurements of banana ashes for the geometry content and per 100 g of banana. In addition, the net count rate obtained for the banana ashes geometry is shown.

Results of the count rate measured for banana ashes (GA2) and banana ashes spiked with KCl (GB2) geometries, 14.18 cps and 18.09 cps respectively, have been significantly higher than the one measured for background (9 cps). Thus, in contrast with crushed banana GMC measurements, it has been possible to use this data for the later activity and total K calculations.

The calibrated detection efficiency for GMC measures of ashes geometry has turned out to be surprisingly high, 99.1%, compared with the radiochemical techniques that have been previously used. Reduction of the geometry size, concretely in height, has caused an increase of gamma emissions detection due to the closer position of the overall ash mass to the detection surface of the instrument. In comparison, the overall crushed banana mass had been disposed along a bigger geometry (500 mL) where gamma emissions from the bottom content had an emission angle that did not enable its detection. In addition, the decrease in sample volume and density by calcination of crushed banana to ashes have represented a decrease in matrix attenuation of the gamma emissions.

For GMC measurements of banana ashes, ^{40}K activity calculated per 100 g of banana have been 11.4 Bq/100 g and the total K concentration deduced from the ^{40}K content has been 374 mg/100 g.

The ^{40}K activity per 100 g of banana obtained for banana ashes matrix GMC measurements has been closer to the ones obtained for LSC and HRGS by banana ashes measures (13.1 Bq/100 g in both cases) than the one obtained for crushed banana measures using HRGS, but equally in the same order of magnitude and hence comparable. Calibration through KCl spiking has resulted to be satisfactory by giving high precision in the results, regardless the high value of measure uncertainty associated to the instrument used.

The total K concentration per 100 g of banana deduced has resulted to be far from the reference value obtained by FAES measurements (496 mg/100) and it has been attributed to the Geiger-Müller instrument, which task is not to accurately analyse radioactive samples but to quickly detect radiation in surfaces due to accidental leakages in a daily basis.

Finally, it has been concluded that GMC can be used for ^{40}K determination in bananas by using a banana ashes matrix to minimise the matrix attenuation effect over gamma emissions and an optimised geometry to ensure the detection of the maximum number of these emissions.

6.6. RADIOCHEMICAL TECHNIQUES COMPARISON

Finally, a discussion over the radiochemical techniques that have been used in this work has been done in order to expose the main advantages and disadvantages of each one and select which suits in different cases.

The main advantages of LSC are the low limit of detection due to the high detection efficiency that provides in the case of a high-energy beta emitter such as ^{40}K , a low background thanks to the lead shielding surrounding the detector and a low measure uncertainty that ensures a high precision between replicates. In contrast, the technique requires an important sample treatment to achieve a clear matrix without interferences, in addition to large times of measurement (easily 40 h for a whole set of standards, samples and blanks) and the difficult access to an ultra low level liquid scintillation spectrometer due to its high cost. Thus, LSC is appropriate for cases where low activity samples are analysed and instruments for sample treatment (such as muffles or sand baths) and measure (1220 Quantulus) are available.

For the case of HRGS, the main advantages of the technique are the few steps needed for sample treatment, allowing to directly measure crushed banana samples obtaining satisfactory results or calcine to ashes for improving the results exactitude; the high selectivity between gamma emissions due to its resolution characteristic of a spectrometric technique and its low background thanks to the shielding surrounding the germanium detector. Instead, it does not have such low limit of detection as LSC and the time of measurement for the sample and the calibration geometries can reach up to 4 days. Hence, HRGS is appropriate for cases of routine measures of samples where sample treatment wants to be skipped for saving time and for not adding uncertainties associated with the treatment procedure in the determination.

Last, GMC presents the advantage of its simplicity when it comes to use it due to its real task of routine measures of working surfaces in radioactive installations, in addition to the little sample treatment needed for the approximate determination of ^{40}K in bananas. In contrast, the technique offers a high measure uncertainty and a high background, which is caused by the null presence of a shielding to reduce the cosmic radiation that is detected along with the sample emissions, in addition to a high limit of detection which forces to have samples with relatively high activity to obtain significant results. Nevertheless, if the purpose of the determination is to teach radiochemistry to students without knowledge in this field, the simple procedure described in this work is entirely valid for ^{40}K determination in bananas.

6.7. BANANA DOSE IN HUMANS

In order to finish this work in the same way it was started, the question of whether the banana consumption is harmful to human health has been answered.

With the banana activity results obtained by measures of banana samples with different radiochemical techniques it has been possible to see that an activity of an average 14 Bq/100 g of banana is not dangerous for humans.

However, an approximation of the effective dose received for a single banana ingest has been calculated and compared with the dose limits established for the average population, for radioactive installations workers and also the considered limit dose for death. The effective dose can be described as the sum of the different weighted equivalent doses in the whole tissues and organs of human body.

Assuming that ^{40}K radiation is caused by electrons (β decay) and photons (γ decay) and this particles mainly affect organs and tissues such as stomach, liver, small intestine, large intestine, kidney, pancreas, spleen, adrenal glands and bones(21), the effective dose calculated is $3 \cdot 10^{-8}$ mSv.

A dose limit of 20 mSv/year is given to workers from a radioactive installation, while for members of the public this value decreases to 1 mSv/year. Moreover, an absorbed dose of 1000-2000 mSv can be deadly in 6 to 8 weeks, while the increase of the dose up to 30000 mSv leads to death in no more than 1 day.

Therefore, with an effective dose of $3 \cdot 10^{-8}$ mSv per banana can be concluded that the human banana intake is completely harmless to health.

7. CONCLUSIONS

After the discussion of the results that have been obtained for ^{40}K determination by the different radiochemical techniques used, the following conclusions have been drawn.

A procedure to determine ^{40}K in bananas has been established comprising the sample treatment of crushed banana and its calcination to ashes, the sample measure by the ^{40}K gamma emissions using HRGS, equipped with an intrinsic germanium detector, in the format of banana ashes matrix placed into an optimised geometry, which has been a 100 mL geometry cover, and the technique calibration by KCl standard spike of a sample geometry.

FAES technique for the reference value obtainment of total K concentration in bananas has been reinforced to be a robust method with low measure uncertainty for the obtention of accurate results.

A procedure for ^{40}K determination by beta emissions has been designed and tested using LSC technique. Accurate results have been obtained by using banana ashes solution with mainly nitric acid and the subsequent calibration for matrix quenching effects by using nitromethane, finally establishing a constant detection efficiency. The technique has provided high precision and the possibility to work with low activity samples, which can be a crucial factor whether the experiment can not be performed with a big quantity of bananas as it has been in this case.

Finally, a simple procedure for ^{40}K determination in bananas has been designed and applied for its future implementation in radiochemistry teaching environments. GMC measurements of banana ashes in an optimised geometry with a calibration through KCl spike have given significantly higher count rates than the background for the posterior ^{40}K concentration calculation, whose result has been quiet satisfactory if the purpose of the determination is to teach students without radiochemistry knowledge.

8. REFERENCES AND NOTES

1. WHO | Development of WHO nutrition guidelines. WHO 2018 [cited 2019 Jun 2]; Available from: https://www.who.int/elena/about/guidelines_process/en/
2. Ministerio de Agricultura, Pesca y Alimentación, Gobierno de España. Estudio del Mercado del Plátano en España y Portugal. 2002 [cited 2019 Apr 15]. Available from: https://www.mapa.gob.es/es/alimentacion/temas/consumo-y-comercializacion-y-distribucion-alimentaria/platano_espana_tcm30-89322.pdf
3. Hardisson A, Rubio C, Baez A, Martin M, Alvarez R, Diaz E. Mineral composition of the banana (*Musa acuminata*) from the island of Tenerife. *Food Chem.* 2001;73(2),153–61.
4. U.S Department of Agriculture (USDA). Food Composition Databases Show Foods -- Bananas, raw. 2016 [cited 2019 Feb 27]. Available from: <https://ndb.nal.usda.gov/ndb/foods/show/09040?fgcd=&manu=&format=Full&count=&max=25&of fset=&sort=default&order=asc&qlookup=09040&ds=&qt=&qp=&qa=&qn=&q=&ing=>
5. Ortega Aramburu X, Jorba Bisbal J. Las Radiaciones ionizantes: utilización y riesgos I. Edicions UPC. 1996.
6. Audi G, Bersillon O, Blachot J, Wapstra AH. The NUBASE evaluation of nuclear and decay properties. [cited 2019 Apr 2]. Available from: <http://csnwww.in2p3.fr/AMDC/>
7. Bé MM, Chisté V, Dulieu C, et al. Monographie BIPM-5, Table of Radionuclides. Bureau International des Poids et Mesures, Sèvres, França. 2010;5, 7-12. Available from: http://www.bipm.org/utls/common/pdf/monographieRI/Monographie_BIPM-%0A5_Tables_Vol7.pdf
8. Bagán H. Millora de la selectivitat en la determinació de radionúclids per escintil·lació plàstica sense generació de residus. Doctoral Thesis. Universitat de Barcelona; 2011.
9. Thomson J. Use and preparation of quench curves in LSC. 2004;1–7.
10. L'Annunziata MF. Handbook of Radioactivity Analysis 3rd Edition. Academic Press; 2012.
11. Radiological Society of North America I. Patient Safety - Radiation Dose in X-Ray and CT Exams. 2019 [cited 2019 Apr 18]. Available from: <https://www.radiologyinfo.org/en/info.cfm?pg=safety-xray>
12. AOAC. Official methods of analysis. Assoc Anal Communities. 1995;1(5),141–4.
13. Sanchez-Castillo CP, Aguirre A, Escamilla I, et al. The mineral content of mexican fruits and vegetables. *J Food Compos Anal.* 2002;11(4),340–56.
14. Miller-Ihli NJ. Atomic absorption and atomic emission spectrometry for the determination of the trace element content of selected fruits consumed in the United States. *J Food Compos Anal.* 1996;9(4),301–11.
15. Guiteras J, Rubio R, Fonrodona G. Curso Experimental En Química Analítica. Síntesis SA. 2003. 214–217.
16. Tahvonen R. Contents of selected elements in some fruits, berries, and vegetables on the finnish market in 1987-1989. *Journal of Food Composition and Analysis.* 1993;6,75–86.
17. Verrezen F, Loots H, Hurtgen C. A performance comparison of nine selected liquid scintillation cocktails. *Appl Radiat Isot.* 2008;66(6–7),1038–42.
18. Luisa Casallas. Evaluación del análisis fisicoquímico del banano común (*Musa sapientum* L) transformado por acción de la levadura *Candida guilliermondii*. 2015;15-21. Available from: <https://www.javeriana.edu.co/biblos/tesis/ciencias/tesis605.pdf>

19. Asociación de Organizaciones de Productores de Plátano de Canarias (ASPROCAN). Información Nutricional - Plátano de Canarias. [cited 2019 Mar 8]. Available from: <https://platanodecanarias.es/nuestros-platanos/informacion-nutricional/>
20. Tarancón A, Bagán H, García JF. Plastic scintillators and related analytical procedures for radionuclide analysis. *J Radioanal Nucl Chem.* 2017;314(2),555–72.
21. España. Real Decreto 783/2001, de 6 de julio, por el que se aprueba el Reglamento sobre protección sanitaria contra radiaciones ionizantes. *Boletín Oficial del Estado*, 26 de julio de 2001, núm. 178, pp. 27284 a 27393.

9. ACRONYMS

| | |
|--------|---------------------------------------------------------|
| A | Mass number |
| BED | Banana Equivalent Dose |
| CAT | Computerized Axial Tomography |
| EC | Electron Capture |
| FAES | Flame Atomic Emission Spectroscopy |
| FAO | Food and Agriculture Organization of the United Nations |
| GM | Geiger-Müller |
| GMC | Geiger-Müller Counting |
| HRGS | High Resolution Gamma Spectroscopy |
| IR | Infrared |
| LOD | Limit of Detection |
| LS | Liquid Scintillation |
| LSC | Liquid Scintillation Counting |
| MCA | Multichannel Analyser |
| PMT | Photomultiplier Tube |
| RSD | Relative Standard Deviation |
| SQP(E) | Spectral Quench Parameter of the External Standard |
| UV | Ultraviolet |
| WHO | World Health Organization |
| Z | Atomic number |

APPENDICES

APPENDIX 1: DIAGRAM OF THE WORK

Figure A1 shows the steps that have been followed in this work, from the initial raw bananas sample to the ^{40}K determinations by different radiochemical techniques, going through all the sample treatment procedures in order to achieve a suitable matrix.

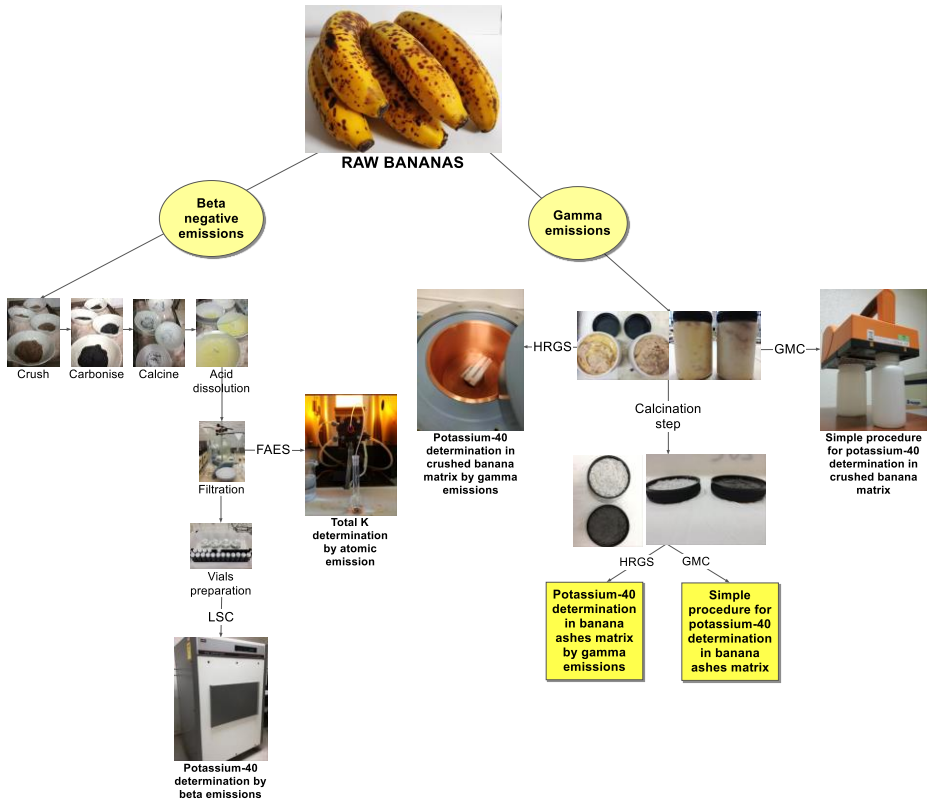


Figure A1. Diagram of all the procedures involved in the work.

APPENDIX 2: LSC CALIBRATION WITH CH_3NO_2

Figure A2 shows the SQP(E) values of standards proportioned by the instrument and the corresponding detection efficiencies calculated. Quench curve is explained in Section 6.3.

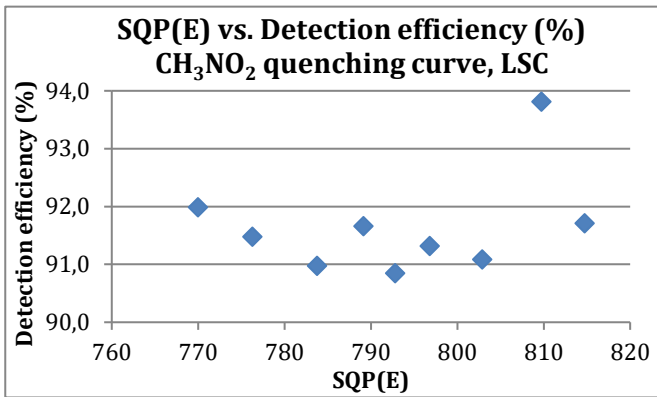


Figure A2. SQP(E) quench calibration curve for increasing volumes of CH_3NO_2 .

Figure A3 shows the spectra obtained for standard vials prepared with increasing volumes of CH_3NO_2 , explained in Section 6.3.

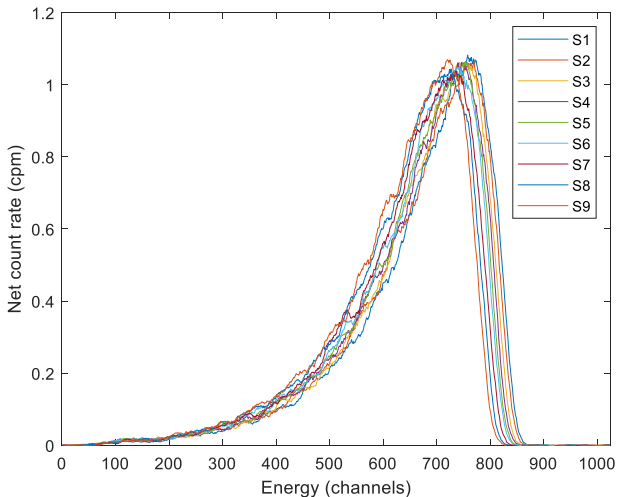


Figure A3. Spectra of the energy in every channel in front of the count rate of the standard vials containing CH_3NO_2 , from S1 to S9.

APPENDIX 3: HOMOGENEITY TEST

An homogeneity test over the crushed banana geometry spiked with KCl (GB1) has been performed to ensure that its preparation by addition of consecutive layers of crushed banana and KCl has been correctly done, having an homogeneous distribution between crushed banana and the added KCl to achieve significant results in the posteriors measures by HRGS.

Three 100 mL geometries have been filled up with GB1 content from the top (H1), middle (H2) and bottom (H3) of the geometry and have been measured by HRGS, each one during 1 day. Results obtained are shown in Table A1.

| Geometry | Net count rate (pulses/s) ^(a) |
|----------|---------------------------------------------|
| H1 | $7.82 \cdot 10^{-2}$ |
| H2 | $1.06 \cdot 10^{-1}$ |
| H3 | $1.20 \cdot 10^{-1}$ |

(a) Net count rate has been obtained by subtracting the background contribution to the measure, which turned out to be 1.207 pulses/min.

Table A1. Net count rate obtained for the three geometries of the homogeneity test.

Slightly different net count rates have been obtained for the three homogeneity test geometries, attributable to negligible bigger amounts of KCl in the middle and bottom of the geometry. Hence, the crushed banana geometry spiked with KCl (GB1) has been considered to be homogeneous.

